Space variant PSF parameterization in image space using printed point source arrays on the HiRez PET/CT

Kotasidis, F.A. and Angelis, G.I. and Matthews, J.C. and Lionheart, W.R.B and Reader, A.J

2010

MIMS EPrint: **2015.43**

Manchester Institute for Mathematical Sciences
School of Mathematics

The University of Manchester

Reports available from: http://eprints.maths.manchester.ac.uk/
And by contacting: The MIMS Secretary
School of Mathematics
The University of Manchester
Manchester, M13 9PL, UK

ISSN 1749-9097

Space variant PSF parameterization in image space using printed point source arrays on the HiRez PET/CT

Fotis A. Kotasidis, Georgios I. Angelis, Julian C. Matthews
Imaging, Genomics and Proteomics
Wolfson molecular imaging centre
University of Manchester
Manchester, UK

William R. Lionheart
School of Mathematics
Alan Turing Building
University of Manchester
Manchester, UK

Andrew J. Reader
Brain Imaging Centre
Montreal Neurological Institute
McGill University
Montreal, QC, Canada

***Abstract*—A new practical and computationally efficient method for deriving and applying the space-variant blurring component of the system matrix is proposed and applied to the HiRez PET/CT scanner. The point spread function (PSF) was sampled at 14400 locations within the field-of-view (FOV) using an array of 120 18-F printed point sources. An HP printer was modified to print the sources on a sheet of A4 paper. To provide enough annihilating material for the positrons and move the array accurately within the FOV a Perspex phantom was designed. The reconstructed PSFs were parameterized in image space and modeled with a pair of multidimensional (3-D) Gaussian distributions. Through the fitting of appropriate functions, model parameters were interpolated and extrapolated for the remaining positions in the FOV. Image reconstruction with resolution modeling was implemented using the expectation maximization algorithm (OP-OSEM) and space variant image based convolution operations. Initial analysis shows significant improvements in the resolution using space variant kernels (reduction of FWHM from 5.5mm down to 2mm at 20cm radially). The improvements are more pronounced at the edge of the FOV when compared to the space invariant method where the discrepancy between the measured space variant blurring kernel and the invariant kernel are larger. Using the printer for producing radioactive point sources, the PSF was sampled at 14400 positions in less than 24h. Parameterizing the kernels in image space also provides a computation efficient alternative to projection space PSF parameterization with similar resolution improvements (a uniform resolution of 2mm throughout the FOV) and minimal increase in the reconstruction time.**

Keywords - point spread function; image reconstruction; printed point sources; PET/CT;

I. INTRODUCTION

Positron emission tomography (PET) image reconstruction using statistical methods often provides images with better signal-to-noise ratio (SNR) compared to conventional analytic algorithms since they allow extensive modeling of the emission and detection processes during data acquisition [1]. In common practice an idealized forward and back-projector is used based on a simple line integral model containing only geometric detection probabilities [2],[3]. This model, although computationally simple, fails to take into account physical phenomena like positron range, inter-crystal scatter, crystal penetration and photon non-colinearity. To correct for these effects and accurately model the relationship between image and projection space a blurring component is usually calculated either by analytic derivation [4],[5], Monte Carlo simulations [6],[7] or by measuring the scanner response to a point source at different points in the field-of-view (FOV)[8],[9],[10]. Simulations provide the most flexible approach as the geometric and the blurring components can be separated but again it needs to be validated with real data.

The 3-D sinogram space can be parameterized by an axial, a radial and an angular (azimuthal) coordinate. The PSF blurs the sinogram data in all 3 directions (axial, radial and angular) with the blurring being a function of the radial, axial and tangential position in the FOV with respect to the lines of response (LOR) at a specific projection angle. Scanning a collimated point source at every voxel in the FOV can provide the most accurate results but such an experimental approach is not practical due to the time needed to collect the data. Usually the PSF parameters for every radial, axial and tangential position are calculated based on a limited number of measured point source data by interpolating and extrapolating the parameters for the remaining positions in the FOV. This parameterization results in a multidimensional function with many unknown parameters and usually rotational and translational symmetries are used to reduce the parameters.

A simpler and less computationally intensive approach is to account for the blurring in image space as opposed to projection space [12],[13]. Although this method improves SNR, it is normally implemented using a spatially-invariant kernel which is clearly sub-optimal when applied to a whole body scanner. The parallax error results in a progressively asymmetric blurring kernel in the radial direction with the asymmetry being a function of the radial distance from the centre of the FOV. The use of axial compression (span) in commercial scanners like the HiRez PET/CT, results in axial under-sampling, and an axial and radial dependency of the

978-1-4244-6494-4/10/$26.00 ©2010 IEEE

axial blurring. This dependency is a product of the varying number of axial LORs combined per plane, the ring difference, the gaps between the block rings and the number of segments. To our knowledge such a spatially variant image-based resolution model has not been implemented before.

Using point source data to derive the variant blurring component is a time consuming process requiring complex and expensive equipment. Usually sophisticated robots are employed to accurately position and move the point sources in the FOV [8],[10],[11]. These computer-controlled devices can only position one point source at a time and with the need for high count statistics, there is a compromise between the number of sampled points and the acquisition duration. Recently the method of producing radioactive point sources using a standard inkjet printer has become increasingly popular. Printed point sources have been used primarily in SPECT to produce quality assurance phantoms [14] and recently in PET for resolution measurements [15]. These studies focused on the feasibility of producing such point sources, demonstrating the simplicity of the method and the ability to scan multiple sources within the same scanning session. One complication of positron emitting isotopes is the need for a medium for positron annihilation, without dramatically affecting counting statistics through attenuation.

In this note we propose the use of a space variant image based PSF model on the whole body HiRez PET/CT. The PSFs are parameterized using image space kernels, scanning an array of printed point sources at various positions in the FOV. To accurately position the source array inside the scanner, a novel phantom was designed, made out of tissue equivalent material.

II. MATERIALS AND METHODS

A. Point source production and optimization

An HP 5440 printer was used in order to print radioactive point sources at predefined positions on a sheet of A4 paper. Standard black ink was being mixed with small quantities of ^{18}-F saline solution (0,1-0,2 ml) via injection into a modified cartridge. The sponge and the membrane which controls the ink delivery inside the cartridge were removed to apply ink directly to the reservoir for maximum efficiency. Using a microscope and following decay of the isotope, checks were made to ensure that the radioactivity ink was deposited on the same position on each occasion. Before printing the array, a rectangular block of ink was printed for uniform ink flow.

In order to accurately space the sources, choose the best source dimensions and minimize the acquisition time, an optimization process was used. Point sources with different diameters and various distances between them were scanned at various locations in the FOV. PSF profiles were qualitatively analyzed to determine the zero overlapping spacing between the PSF tails. Point sources of different dimensions were also analyzed by looking at microscope enhanced images and by calculating the activity reproducibility. Based on this optimization, the dimensions of the sources and their spacing were used to design the array in Microsoft publisher.

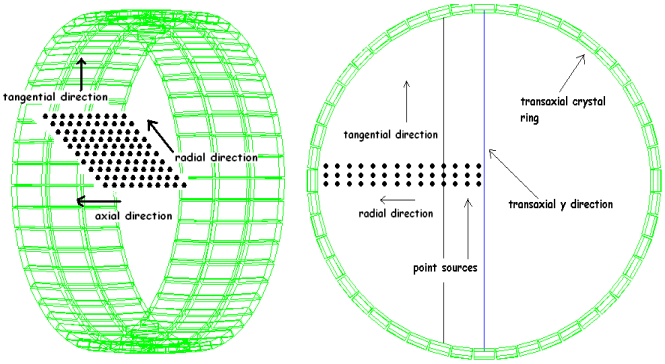

Fig.1 Schematic representation of the sampling scheme that was used inside the FOV. The axial extent of the array covered almost the entire axial FOV and half the transaxial FOV.

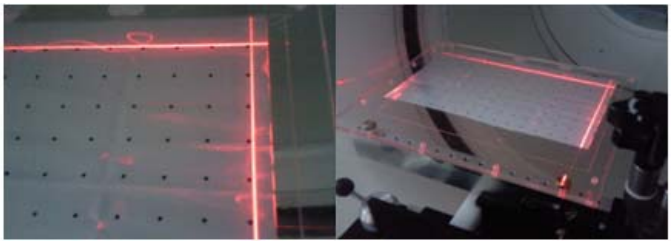

Fig.2 Lasers were used to align the point source array. After setting the zero reference point a topogram CT scan was used to adjust the axial position.

B. Positioning and aligning the point source array

To position the point sources within the FOV and allow them to move in all 3 dimensions (fig.1) a phantom was designed. The phantom was made out of an aluminum bar, located outside the FOV, in which holes were drilled every 2cm. Attached to the bar were 2 sheets, 3mm width each, made out of a tissue equivalent material (Perspex). This width allowed the sheets to be transparent, making positioning and alignment easier. The width of 3mm was chosen as a compromise between positron annihilation and the minimization of attenuation.

To move the phantom within the FOV the aluminum bar was attached to the QC phantom holder which subsequently was attached to the scanner's bed. The phantom holder as well as the holes in the metal bar allowed movement in the radial and tangential direction while the scanner's patient handling system (PHS) was used to cover the axial direction. The point source alignment was done in 2 steps. First the scanners laser system was used to position the sources with a certain degree of accuracy (fig.2). With the sources positioned, quick scans were taken and projection data examined to check the axial deviation of a single line of point sources as it should appear in the same axial plane. Since the sources are accurately aligned to each other, only a single line of sources needs to be aligned with respect to the scanners axis. To further minimize any

positioning errors, changes in the axial position of the point source array were controlled by changing the scanned PET FOV with respect to a low quality CT scan (topogram).

C. *Scanning and reconstruction protocol*

The Biograph 6 Barrel-HiRez PET/CT (Siemens Molecular Imaging Inc., TN, USA) is a whole body scanner capable for list-mode acquisition [8],[16]. The scanner has 3 axial block rings and in every ring 13 axial crystal rings. The spacing between blocks is assumed to be equal to one crystal width, despite the gaps are not being equal in all directions (axially and transaxially). Hence there are another 2 axial rings corresponding to these gaps. The axial extent of the scanner is 16.2 cm and it has 81 direct and cross planes resulting in an axial sampling distance of 2 mm. Compared to the blocks within the central ring the outer ring blocks are positioned at an angle of 7,5 degrees giving a spherical geometry. The block design is made of 13x13 LSO crystals with every crystal being 4x4x20mm. Each block ring has 48 blocks resulting in 624 crystals and 48 gaps per ring. The data are acquired in span 11 with a maximum ring difference of 27. This results in 313 sinograms in 3-D mode (5 segments) with each sinogram consisting of 336 radial elements and 336 angular views.

Each array had a rectangular grid of 8 (axially) x 15 (radially) point sources. Radially the array moved at 4 radial positions with a 5mm step. In each radial position the sources also sampled 3 tangential positions with a sampling distance of 5mm. In the axial direction the lack of axial symmetry results in having to scan at least half the axial FOV. The 8 sources in the axial direction of the sheet covered a distance equal to 16 cm allowing the entire axial FOV (16,2cm) to be scanned with a sampling distance of 2mm at 10 axial positions.

Since the 18-F sources decay fast relative to the scan duration, progressively longer acquisition periods were used at different positions in order to compensate for the radioactivity decay and achieve matched statistics for all the scans. In total this resulted in 14400 point source measurements within a segment of the FOV. Axial and rotational symmetry were exploited to extrapolate the measurement to the entire FOV.

PET data were collected in 32-bit list mode and organized into prompts, randoms and net-true sinograms using an in-house list-mode histogrammer. Fig.3a and 3b show a transaxial and a horizontal section through the 3-D sinogram space. The blurring is immediately apparent towards the edge of the FOV with the point sources shifting in the radial direction at increasing axial distance due to the decreasing ring radius. Standard corrections were applied on the net-true sinogram data (attenuation, normalization and scatter) and an in-house 3D OP-OSEM algorithm with a pre-calculated geometric system matrix, based on the Siddon algorithm, was used to reconstruct the emission images. We avoided the use of the standard HiRez reconstruction software since it uses Fourier re-binning (FORE + 2-D), further blurring the point source data.

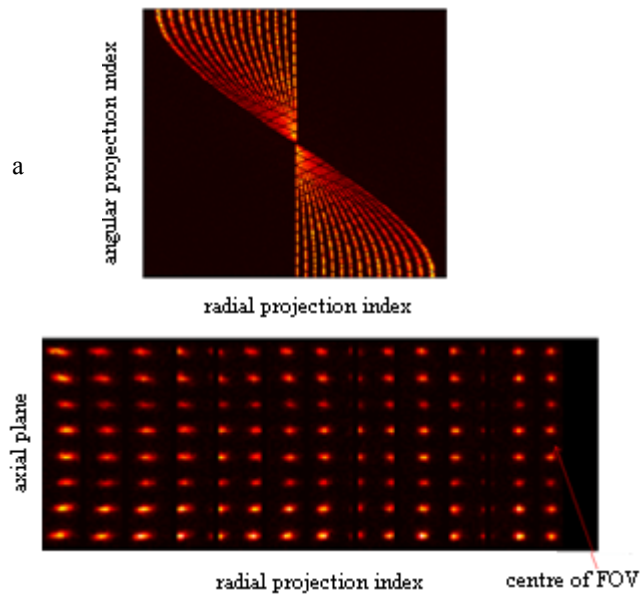

Fig.3 Transaxial a) and horizontal b) section through the 3-D sinogram space. Moving away from the centre of FOV the radial elongation is obvious. The gaps between the crystals are seen as black strips in the axial profile b) especially when an LOR corresponding to a gap passes through a point source.

D. *PSF parameterization and space variant image-based resolution modelling implementation*

As mentioned in the introduction the PSF data can be used directly if sampled for every voxel in the FOV. Since one can only sample the PSF at a finite number of positions, a PSF model was used in order to fit a number of parameters to the measured data. Each reconstructed PSF was represented in image space as a mixture of 2 multidimensional (3-D) Gaussian distributions (radial, axial and tangential components).

$$PSF(x,\theta)=\sum_{i=1}^{2} w_i\, p_i(x,\theta) \tag{1}$$

where

$$p_i(x_j,\theta)=\prod_{j=1}^{3} N(x_j,\ \ _{ij},\sigma_{ij}) \tag{2}$$

and

$$N(x,\ \ ,\sigma)=\frac{1}{(2\pi)^{1/2}\sigma}\exp\left(-\frac{1}{2}\left(\frac{x-}{\sigma}\right)^2\right) \tag{3}$$

with

$$\sum_{i=1}^{2} w_i=1,\quad w_i\geq 0 \tag{4}$$

Where $_{ij}$ and σ_{ij} are the mean and standard deviation for the ith Gaussian distribution and the jth dimension (radial, tangential and axial axes) and w_i is the mixing coefficient for the ith Gaussian distribution.

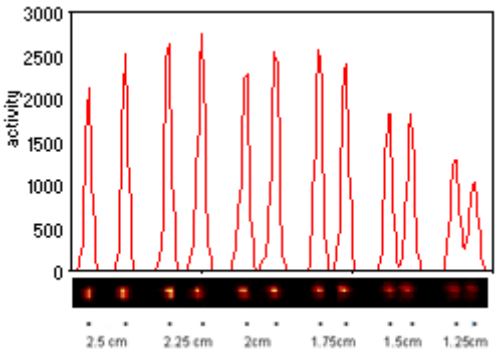

Fig.4 Point Spread Function profiles of varying diameter and spacing. When the spacing of the sources is too close, the distribution tails start to overlap

A total of 13 parameters (6 parameters per Gaussian distribution and one mixing coefficient) where estimated for each measured PSF using an EM algorithm with the covariance matrices restricted to be diagonal. In a second step the derived model parameters were fitted to functions dependent on the radial (r) and axial (z) position of the point source. This enabled determination of the model parameters for every position in the FOV, from which the blurring kernels were calculated and stored for every voxel in image space.

Implementing an image based resolution modeling involves a convolution operation of the current image estimate with a blurring kernel. The transpose of the kernel is applied on the back-projected correction image as well as the sensitivity image. To implement a space variant image based reconstruction a routine was written in Matlab to perform axially and radially variant blurring with the kernel being a function of the voxel position.

E. Evaluation of spatially variant and invariant PSF reconstructions

Point source data were reconstructed using a 336 x 336 x 81 image grid with a 2mm x 2mm x 2mm voxel size. The radial FWHM was calculated as a function of the radial distance using the scanner's software (no PSF modeling), a spatial invariant implementation of resolution modeling using a kernel matching the one in the centre of the FOV (4.3mm fwhm) and with the space variant method.

III. RESULTS

A. Point source production and optimization

Fig.4 shows the profiles from an axial slice through a reconstructed volume with the point sources spaced at decreasing distances toward the edge of the FOV. As the distance between the sources decreases the PSF tails start to overlap. For sources spaced evenly at intervals of 1.5cm are sufficient to differentiate adjacent PSFs but a more conservative approach was used with a 2 cm spacing for all the scans. A source diameter of 2mm was chosen matching the dimensions of the reconstructed voxels. Furthermore using enlarged images from a microscope we observed ink droplets being printed outside the point source boundaries for sources smaller than 2mm. To further increase the activity per source we printed the array multiple times. After 7 reprints a total activity of 48-52 MBq per array was achieved and this configuration was used for all the scans.

B. Positioning and aligning the point source array

To find the most suitable material for the array sheets the attenuation coefficient at 511keV was calculated for a number of materials. Perspex was chosen as it has almost equivalent attenuation properties with water and adipose tissue. As the ^{18}F positron range is around 1mm, a 3mm width per sheet was chosen in order to maximize counting statistics with minimal attenuation. In order to quantify the loss of counts through attenuation we calculated the attenuation loss fraction as a function of the photon incidence angle to the Perspex sheet. For photons hitting the Perspex surface at a small angle (up to 60 degrees) the attenuation probability is kept below 0.2. The average attenuation loss fraction was found to be 0.21.

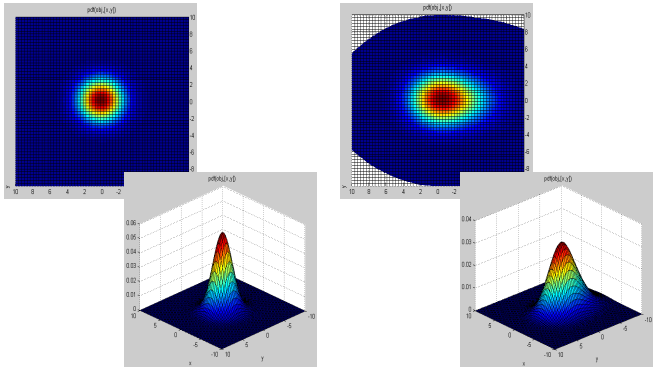

Fig.5 Fitted PSFs at 2cm (left) and 22cm (right) from the centre of the FOV. Close to the centre of the FOV the PSF is almost symmetric while at the edge of the FOV the radial elongation results in an asymmetry in the distribution

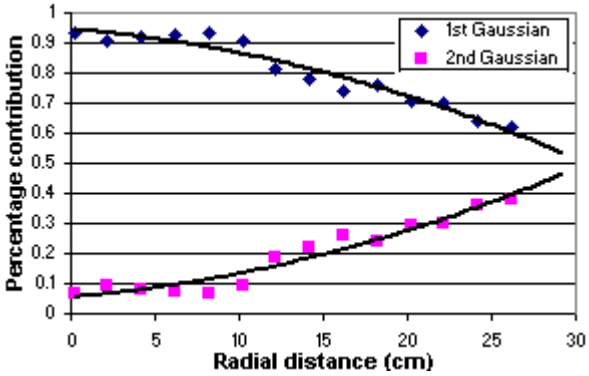

Fig.6 Mixing proportions between the Gaussian distributions. The second Gaussian fits the tail of the PSF which becomes prominent at increasing distance due to the PSF radial elongation

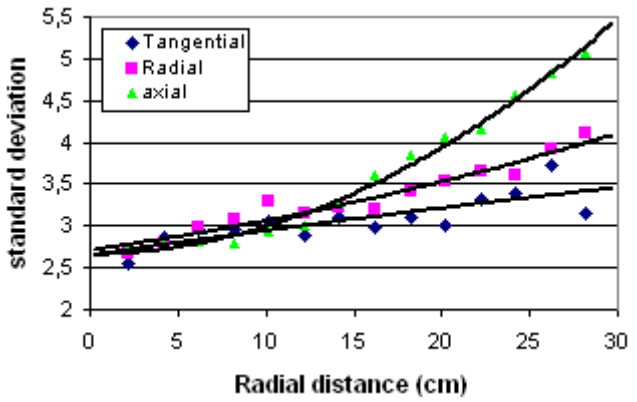

Fig.7 Radial and tangential standard deviation for the first Gaussian component as a function of the radial distance. The PSFs were reconstructed on a 1008x1008x243 image grid for finer data sampling with a voxel size of 0.66mm x 0.66mm x 0.66mm

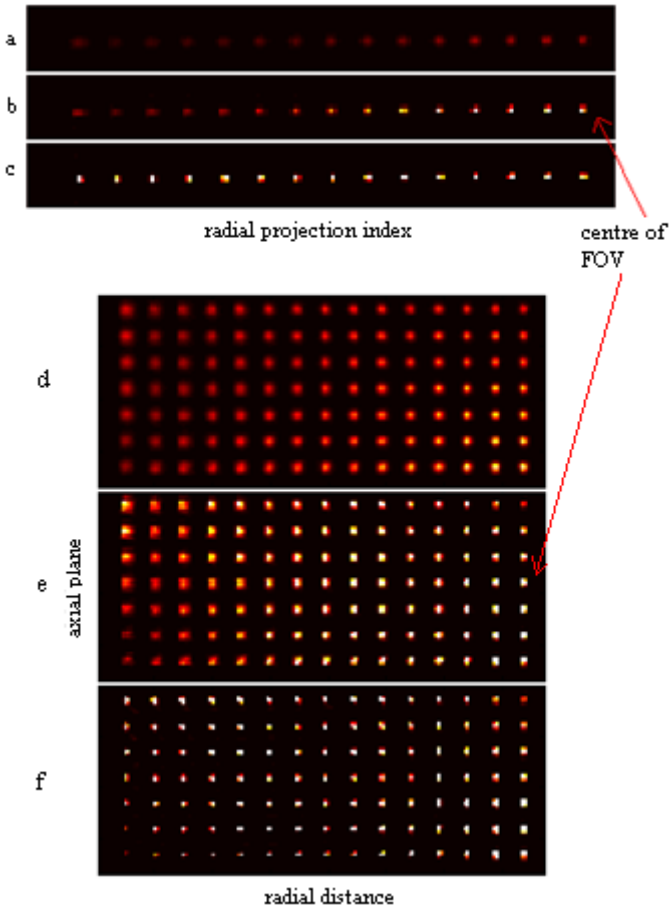

Fig.8 transaxial (a,b,c) and horizontal (d,e,f) sections through images reconstructed with no PSF (a,d), with a spatially invariant kernel (b,e) and with the proposed space variant PSF model (c,f).

C. *PSF parameterization*

Fig 5 shows 2-D sections through the 3-D fitted PSFs at 2 positions near the centre and near the edge of the FOV. The asymmetry in the distribution is immediately apparent in the radial direction. As mentioned before this is modeled by using 2 Gaussians, with their mixing proportions being a function of the radial coordinate as seen in Fig.6. The proportions of the second Gaussian which accounts for the PSF tails is increasing as a function of distance from the centre of the FOV with the mixing proportions being almost equal at the edge of the FOV. Looking at the standard deviation graph as a function of the radial distance the axial component has the biggest blurring followed by the radial and tangential components (Fig.7). This is expected due to the increased axial under-sampling (span 11) that is used during binning of the list-mode data.

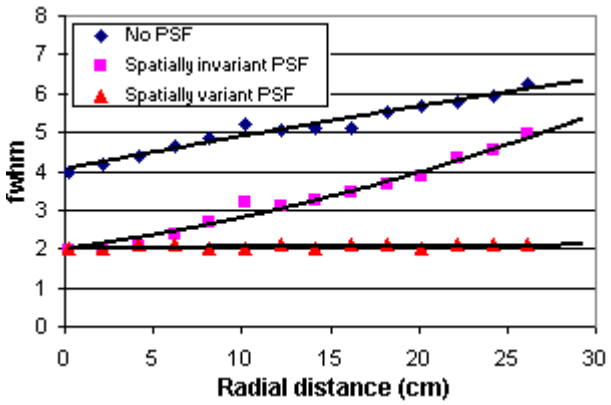

Fig.9 Radial FWHM with and without resolution modeling as a function of radial distance from the centre of the FOV

D. *Evaluation of point source data on the HiRez*

Point source data were reconstructed using: the scanner's reconstruction software, an image based PSF reconstruction with a stationary kernel and the space variant image based method. The use of the space invariant PSF model results in a dramatic increase in the recovered activity. The improvement is more pronounced in the centre of the FOV (Fig.8) as the used kernel matches the scanner's blurring in that point (4.3mm fwhm). Moving to the space variant reconstructed point sources and comparing it with the invariant method the largest changes as expected are located towards the edge of the FOV. Fig.9 shows the radial resolution for all the methods. Using a spatially variant resolution model a uniform resolution of 2mm is achieved both in the radial, axial and tangential direction. At 20cm from the centre the space-invariant model improved FWHM resolution radially up to 32% (from 5.5mm to 3.7mm) with the space-variant method improving resolution up to 70% (from 5.5mm to 2mm) similar to [7].

IV. Discussion – Conclusion

This work proposes the use of a space variant resolution model using image space PSF parameterization and applied to the HiRez whole-body PET/CT. To derive the blurring kernels we used printed point source arrays along with a Perspex phantom. Using this method to sample the PSF at various

positions provides an excellent alternative to the previously used computer controlled devices. The large number of point sources that can simultaneously be scanned allowed us to use a very fine sampling scheme, with minimal impact on the acquisition time. The total acquisition time was estimated to be 24 hours split between 6 scanning sessions as after 4 hours of scanning the acquisition time becomes significant due to decay. This methodology for sampling the PSF provides far more scanned points in considerably less time compared to using robotic equipment for data acquisition. In addition it is easier to design and far less expensive.

The addition of a resolution model in the reconstruction dramatically improves the resolution properties of the images. The proposed space variant image based resolution modeling method demonstrates resolution improvements similar to projection space resolution modeling methods without requiring detailed knowledge of the scanner geometry. Comparing the image based methods, even at 10 cm from the centre of the FOV (where most main body organ are located), the addition of a variant kernel compared to a stationary one can improve resolution more than 1mm. This is of particular importance for detecting small tumors in clinical oncology scans.

Rotational symmetry of the model was assumed as this has been validated for the specific scanner [8]. Using spatially-variant kernels also results in the convergence being space variant with the centre of the FOV converging more quickly compared to the edge of the FOV. This also has a direct impact on the spatial characteristics of noise which will be the subject of future investigations. Overall using a spatially-variant model as opposed to an invariant model produces point sources images with a uniform resolution across the reconstructed FOV.

ACKNOWLEDGMENT

The authors would like to thank P. Noonan for his help in setting up the printer apparatus and the WMIC cyclotron team for the constant and reliable ^{18}F production.

REFERENCES

[1] J. Qi, R. Leahy, S. Cherry, A. Chatziioannou, and T. Farquhar, "High-resolution 3-D Bayesian image reconstruction using the microPET small-animal scanner," Phys. Med. Biol., vol. 43, pp. 1001–1013, 1998.

[2] P. M. Joseph, "An improved algorithm for reprojecting rays through pixel images," IEEE Trans. Med. Imag., vol. MI-1, pp. 192–196, 1982.

[3] F. Jacobs, E. Sundermann, B. De Sutter, M. Christiaens, I. Lemahieu, "A fast algorithm to calculate the exact radiological path through a pixel or a voxel space" , CIT. Journal of computing and information technology ISSN 1330-1136, 1998, vol. 6, no1, pp. 89-94 (7 ref.)

[4] A. Rahmim, J. Tang, M. A. Lodge, S. Lashkari, M. R. Ay, R. Lautamaki, B.M.W.Tsui,andF.M.Bengel "Analytic system matrix resolution modeling in PET: an application to Rb-82 cardiac imaging" Phys. Med. Biol., vol. 53, pp. 5947-5965, 2008.

[5] S. Moehrs, M. Defrise, N. Belcari, A. Del Guerra, A. Bartoli, S. Fabbri, G. Zanetti, "Multi-ray-based system matrix generation for 3D PET recosntruction" Phys. Med. Biol. 53 (2008) 6925–6945

[6] P. Alessio, P. Kinahan, T. Lewellen. "Modeling and incorporation of system response functions in 3-D whole body PET". IEEE Trans Med Imaging. 2006; 25:828–837.

[7] J. E. Ortu˜no, P. Guerra, J. L. Rubio, G. Kontaxakis, and A. Santos, "3D OSEM-based iterative image reconstruction for high resolution PET using precalculated system matrix," Nuclear Instruments and Methods in Physics Research Section A, vol. 569, no. 2, pp. 440–444, 2006.

[8] V. Panin, F. Kehren, C Michel, M Casey. "Fully 3-D PET reconstruction with system matrix derived from point source measurements". IEEE Trans Med Imaging. 2006;25:907–921.

[9] E. De Bernardi, M. Mazzoli, F. Zito, G. Baselli. "Resolution recovery in PET during AWOSEM reconstruction: a performance evaluation study", IEEE Trans. Nucl. Sci., 54 (5), pp. 1626-1638, 2007

[10] Wiant, David B.; Gersh, Jacob A.; Bennett, Marcus C.; Bourland, J. Daniel; "PET image reconstruction using LOR-OSEM with a 3D spatially variant system matrix'', ,MNuclear Science Symposium Conference Record (NSS/MIC), 2009 IEEE , pp. 3752 – 3758,2009

[11] M. Tohme, J. Qi. "Iterative image reconstruction for positron emission tomography based on a detector response function estimated from point source measurements" Phys. Med. Biol. 54 3709–25

[12] A. J. Reader, P. J. Julyan, H. Williams, D. L. Hasting, and J. Zweit, "EM algorithm system modeling by image-space convolution technique for PET reconstruction," IEEE Trans. Nucl. Sci., vol. 50, no. 5,pp. 1392–1397, Oct. 2003.

[13] F. Sureau, A. Reader, C Comtat, C. Leroy, M. Ribeiro, I. Buvat, "Impact of image-space resolution modeling for studies with the high-resolution research tomograph". J Nucl Med 2008;49:1000 doi:10.2967/jnumed.107.045351.

[14] J. Van Staden, H. du Raan, M. Lötter, A. van Aswegen, C. Herbst "Production of radioactive quality assurance phantoms using a standard inkjet printer". Phys Med Biol 52:N329–337

[15] V. Sossi, K. R. Buckley, P. Piccioni, A. Rahmim, M.-L. Camborde, and T. J. Ruth, "Printed sources for positron emission tomography (PET),"in Proc. IEEE NSS and MIC 2003 Conf. Rec., Portland, OR, Oct. 2003.